THE JOURNAL OF PHYSICAL CHEMISTRY A

 VOLUME 111, NUMBER 21, MAY 31, 2007

ARTICLES

Theoretical and Experimental Investigations of the Electronic Rydberg States of Diazomethane: Assignments and State Interactions

Igor Fedorov, Lucas Koziol, Guosheng Li, Jessica A. Parr, Anna I. Krylov, and Hanna Reisler*

Department of Chemistry, University of Southern California, Los Angeles, California 90089-0482

Received: February 26, 2007; In Final Form: March 16, 2007

The electronic states of diazomethane in the region 3.00−8.00 eV have been characterized by ab initio calculations, and electronic transitions in the region 6.32−7.30 eV have been examined experimentally using a combination of 2 + 1 REMPI spectroscopy and photoelectron imaging in a molecular beam. In the examined region, three Rydberg states of 3p character contribute to the transitions, $2^1A_2(3p_y \leftarrow \pi)$, $2^1B_1(3p_z \leftarrow \pi)$, and $3^1A_1(3p_x \leftarrow \pi)$. The former two states are of mostly pure Rydberg character and exhibit a resolved *K* structure, whereas the $3^1A_1(3p_x \leftarrow \pi)$ state is mixed with the valence $2^1A_1(\pi^* \leftarrow \pi)$ state, which is unbound and is strongly predissociative. Analyses of photoelectron kinetic energy distributions indicate that the ground vibrational level of the $2^1B_1(3p_z)$ state is mixed with the $2^1A_2(3p_y)$ ν_9 level, which is of B_1 vibronic symmetry. The other $2^1A_2(3p_y)$ vibronic states exhibit pure Rydberg character, generating ions in single vibrational levels. The photoelectron spectra of the $3^1A_1(3p_x \leftarrow \pi)$ state, on the other hand, give rise to many states of the ion as a result of strong mixing with the valence state, as evidenced also in the ab initio calculations. The equilibrium geometries of the electronic states of neutral diazomethane were calculated by CCSD(T), using the cc-pVTZ basis, and by B3LYP, using the 6-311G(2df,p) basis. Geometry and frequencies of the ground state of the cation were calculated by CCSD(T)/cc-pVTZ, using the unrestricted (UHF) reference. Vertical excitation energies were calculated using EOM-CCSD/6-311(3+,+)G* at the B3LYP optimized geometry. The theoretical results show that the $2^1A_2(3p_y \leftarrow \pi)$ and $2^1B_1(3p_z \leftarrow \pi)$ states have geometries similar to the ion, which has C_{2v} symmetry, with slight differences due to the interactions of the electron in the 3p orbital with the nuclei charge distributions. The geometry of the $3^1A_1(3p_x \leftarrow \pi)$ state is quite different and has C_s symmetry. The experimental and theoretical results agree very well, both in regard to excitation energies and to vibrational modes of the ion.

1. Introduction

Diazo compounds serve as sources of carbenes in organic synthesis and participate in alkylation reactions.[1] Diazomethane is an important source of methylene, and its photochemistry is relevant to understanding the chemistry in atmospheres rich in N_2 and methane, such as in Titan, Triton, and Pluto.[2] Not surprisingly, elucidating its excitation and fragmentation mechanisms has attracted interest since 1933.[3] In spite of this interest, its excited electronic states have not been fully assigned. The reason is, of course, the instability of diazomethane and its explosive nature. The C−N bond is weak: the dissociation energy to triplet me-

* Corresponding author. E-mail: reisler@usc.edu.

10.1021/jp071590r CCC: $37.00
Published on Web 05/05/2007

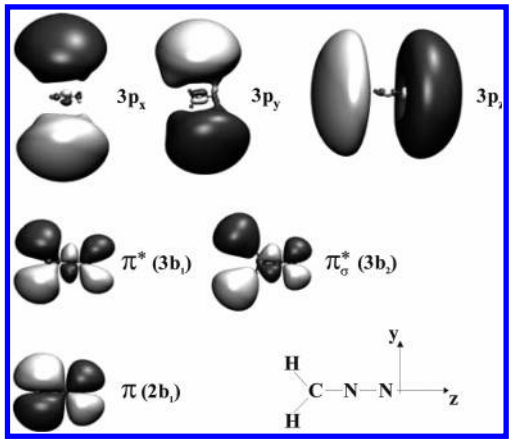

Figure 1. Molecular orbitals relevant to ground and excited electronic states of CH_2N_2.

thylene is <38 kcal/mol and to singlet methylene it is <47 kcal/mol,[1,4] and the molecule is unstable. The goal of the present paper is to characterize the electronic structure and photophysics of diazomethane in the region of its lowest Rydberg states by using a combination of high-level electronic structure calculations and photoelectron and photofragment ion imaging experiments. This would aid, among others, in developing sensitive spectroscopic diagnostics for diazomethane via its Rydberg states. Therefore, our focus is also on identifying electronic state interactions and estimating dissociation rates.

The electronic configuration of ground state diazomethane (1^1A_1) is:

$$[\text{core} + \text{low-lying}]^{16}(7a_1)^2(2b_2)^2(2b_1)^2(3b_2)^0(8a_1)^0(3b_1)^0 =$$

$$[\text{core} + \text{low-lying}]^{16}(\sigma)^2(\pi_\sigma)^2(\pi)^2(\pi_\sigma^*)^0(\sigma^*)^0(\pi^*)^0$$

where "low-lying" refers to the 1s core orbitals, two σ_{CN} orbitals, as well as one extended sigma-bonding and two π-type molecular orbitals (which are not involved in excitations). Relevant molecular orbitals are shown in Figure 1. CH_2N_2 lies in the *yz* plane, with the *z*-axis coinciding with the C_2 symmetry axis (CNN bond). The lowest valence excitations promote an electron from the π orbital to the π^* or π_σ^* orbital.[5] Because the ionization energy (IE) of diazomethane is low (experimentally determined at 9.00 eV),[6] the 3s, 3p, and 3d Rydberg states are located in the same region as the valence states.[6] The ion's excited states are at 14.13 and 15.13 eV, and the parent ion is quite stable.[6]

The most intense electronic transition of diazomethane is $2^1A_1 \leftarrow 1^1A_1$ ($\pi^* \leftarrow \pi$). The antibonding character of the target molecular orbital makes this state unbound, dissociating adiabatically to $N_2(^1\Sigma_g^+) + CH_2(\tilde{c}^1A_1)$, in agreement with Herzberg's observations.[7,8] As of yet, the Rydberg states have not been fully characterized. An earlier theoretical study estimated them to lie vertically at 5.89 (3s), 6.65−6.87 (3p), and 7.48−7.68 (3d) eV.[5] However, the proximity of valence states can lead to interactions with core electrons, giving rise to valence/Rydberg character and affecting quantum defects. A more recent study suggested that all states at 5.31−7.29 eV contain some Rydberg character and that the 2^1A_1 ($\pi^* \leftarrow \pi$) state, found at 5.53 eV vertically, is mostly valence and has the largest oscillator strength.[9]

Absorption spectra identify the strongest absorption at 260−190 nm (4.77−6.53 eV), a region that includes the intense $2^1A_1 \leftarrow 1^1A_1$ ($\pi^* \leftarrow \pi$) transition.[10,11] The absorption exhibits diffuse structures at 230, 218, and 214 nm, which may belong to several mixed valence/Rydberg states. At yet shorter wavelengths (154−193 nm), Merer observed in absorption a series of perpendicular bands, which he characterized as having $^1B_1$ and $^1B_2$ symmetry.[12] Some had a resolved *K* structure, whereas others were more diffuse. Specifically, in the region near 190 nm, he assigned the bands to transitions to three Rydberg states, most probably 3p, which he denoted D($^1B_1$), E($^1B_2$), and F($^1B_1$). He also identified perturbations among some of these states and attributed them to Coriolis coupling. In addition, two intense and diffuse band systems, which do not fit any Rydberg series, are centered at 175 and 140 nm and may indicate mixed states containing a large contribution of valence $\pi^* \leftarrow \pi$ excitations.[9,12]

To date, no molecular beam studies of diazomethane have been reported because of difficulties in preparing and delivering it intact into the interaction chamber. In an attempt to develop efficient sources of carbenes, we have recently adapted the traditional MNNG (*N*-methyl-*N*′nitro-*N*-nitrosoguanidine) + KOH preparation method of diazomethane[13,14] for work in molecular beams. We also modified our inlet and pulsed-nozzle systems for stable and safe delivery.

We have used 2 + 1 resonance enhanced multiphoton ionization (REMPI) complemented by photoelectron imaging of the excited states to characterize Rydberg states in the region around 190 nm previously studied by Merer.[12] We have obtained REMPI and photoelectron spectra and identified intense, *K*-resolved transitions not seen in the one-photon absorption experiments of Merer. We assign them to the $2^1A_2 \leftarrow 1^1A_1$ ($3p_y \leftarrow \pi$) Rydberg transition allowed only in two-photon absorption. Moreover, we obtain for the first time photoelectron spectra from excited states of diazomethane. These spectra reveal interactions between electronic states. The accompanying high-level electronic structure calculations reported here determine ground, Rydberg, and ionic state geometries and vertical transition energies. Combined with experiments, they enable us to characterize the nature of the excited electronic states and their interactions.

Our results show that the observed transitions in the region 51 000−58 900 cm^{-1} (6.32−7.30 eV) can be assigned to three electronic Rydberg states: the $2^1A_2(3p_y \leftarrow \pi)$ state, which can be excited by a two-photon transition, and the $2^1B_1(3p_z \leftarrow \pi)$ and $3^1A_1(3p_x \leftarrow \pi)$ states, which can be accessed by both one- and two-photon transitions. We show that specific vibronic levels of the Rydberg $2^1A_2(3p_y)$ and $2^1B_1(3p_z)$ states interact due to accidental resonances. In addition, we find that the Rydberg $3^1A_1(3p_x)$ wavefunction is strongly mixed with a dissociative valence $2^1A_1(\pi^* \leftarrow \pi)$ state. We propose that the one-photon absorptions seen by Merer in this wavelength region are due primarily to vibrational progressions in the $2^1B_1(3p_z)$ state and that some levels are mixed with the $2^1A_2(3p_y)$ state, which is dark in one-photon excitation. In a future paper, we will report assignments of other vibronic levels of the excited Rydberg states of diazomethane and its isotopologs and compare them to vibrational states of the ground state ion. The complete vibronic analysis confirms the assignments proposed in this paper.

2. Experimental Details

The experimental arrangement has been described before,[15,16] and only relevant experimental details are presented here. In particular, we describe the synthesis of CH_2N_2, a reactive and explosive compound, and its transport to the molecular beam without decomposition.

For CH_2N_2 synthesis, an all-glass vacuum line, constructed of greaseless Teflon high vacuum valves and O-ring joints, was

used. This line consisted of three sections: a reactor, two traps, and a vacuum manifold. The reactor was fitted with a pressure-equalized addition funnel. CH_2N_2 was prepared under vacuum by the reaction of 2.6 g of *N*-methyl-*N*′-nitro-*N*-nitrosoguanidine (TCI America) with an excess of aq ~15 mL of NaOH (2.5M). The resulting CH_2N_2 was purified by passing the gas through two traps held at −78 °C (195 K) with a dry ice/ethanol slush and collected in a 12 L glass flask housed in a steel mesh box and protected from exposure to light. The pressure of CH_2N_2 is kept less than 30 Torr; otherwise it will begin to condense in the dry ice/ethanol traps, where it is likely to explode. The IR and UV spectra of CH_2N_2 prepared by this procedure were in good agreement with published spectra[10,11,17,18] and contained negligible amounts of impurities. The sample survived for several days until it was depleted by use.

A molecular beam of CH_2N_2 was obtained by supersonic expansion of a gaseous mixture containing ~1.5% CH_2N_2 in helium at a backing pressure of 2 atm into the source chamber. This mixture was introduced into the source chamber through a pulsed piezoelectric nozzle (10 Hz, diameter 0.5 mm), and the molecular beam was skimmed before entering the ionization chamber. Because CH_2N_2 decomposes on metallic surfaces, metal parts of the pulsed nozzle making contact with the gas mixture were replaced with fiberglass-reinforced polyetherimide (Ultem 3040). Black nylon tubing was used to make connections. The rotational temperature of the skimmed molecular beam was not determined directly, but based on expansion conditions and previous results, it is estimated to be ~10 K.

We wish to emphasize that CH_2N_2 is a toxic and hazardous gas, which can decompose explosively and spontaneously, and thus appropriate safety precautions must be taken. CH_2N_2 should be handled only at low pressures and on a small scale. At no time should the gas be allowed to condense into the liquid phase. Throughout our experiments, a pressure of 25 Torr was never exceeded. Safety equipment (safety shields, safety glasses, face shields, leather gloves, and protective clothing such as leather suits, Kevlar sleeves, and earplugs) must be used at all times. Care must be taken to avoid known triggers of CH_2N_2 decomposition such as intense light, exposure to rough, metallic, or acidic surfaces, and abrupt changes in temperature, pressure, and phase.

To characterize the excited states of CH_2N_2 in the region 51 000−58 900 cm^{-1} (6.32−7.30 eV), two types of experiments were carried out. In the first set, CH_2N_2 was excited by a resonant two-photon transition at 51 000−58 900 cm^{-1} (6.32−7.30 eV) and ionized by absorbing nonselectively another photon of the same wavelength. A 2 + 1 REMPI spectrum was recorded by monitoring the signal from the parent ion (m/e = 42) as a function of laser excitation wavelength. The tunable UV laser beam (0.7−1.0 mJ focused by a 45 cm focal length lens) was generated by frequency doubling (Inrad Autotracker III) the linearly polarized output of a Nd:YAG (Spectra Physics GCR230) laser pumped dye laser system (Continuum ND6000, LDS 751, 25−30 mJ). No attempt was made to normalize the spectrum (the laser power varied by ± 30%). Ions produced in the ionization chamber were extracted and accelerated by three-stage ion optics into a linear time-of-flight (TOF) mass spectrometer. Only ions of m/e = 42 ($CH_2N_2^+$) were detected using a 42 mm diameter microchannel-plate (MCP) detector with a coupled phosphor screen (Burle Electro-optics, Inc.). The ion optics and TOF region were shielded from magnetic fields by a μ-metal tube. Signals from the MCP were amplified, collected with a digital oscilloscope (Tektronix TDS 3054), and transferred to a PC for analysis.

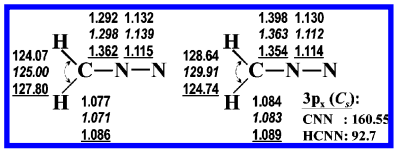

Figure 2. Left panel: Ground state equilibrium structures (Å and deg) of CH_2N_2 for: the neutral (1^1A_1) at CCSD(T)/cc-pVTZ (regular print) and B3LYP/6-311G(2df,p) (italics) and for the cation ($1^2B_1(\infty \leftarrow \pi)$) at CCSD/6-311G** (underlined). The corresponding nuclear repulsion energies are: 61.280112, 61.514227, and 61.118198 hartrees, respectively. Right panel: Excited state equilibrium structures for the 2^1A_2-($3p_y \leftarrow \pi$), $2^1B_1(3p_z \leftarrow \pi)$, and $3^1A_1(3p_x \leftarrow \pi)$ states shown in normal, italics, and underlined print, respectively. CNN and HCNN refer to respective angle and dihedral angle for the C_s $3^1A_1(3p_x \leftarrow \pi)$ state. The corresponding nuclear repulsion energies are: 60.705257, 59.502297, and 60.715012 hartrees. Experimental parameters of ground state: CN length: 1.300 Å; NN length: 1.139 Å; CH length: 1.075 Å; HCH angle: 126.0°.

TABLE 1: Vertical Excitation Energies (ΔE_{vert}, eV), Oscillator Strengths (f_L), Dipole Strengths (μ^2_{tr}, au), and Changes in Second Dipole Moment of Charge Distributions ($\Delta\langle R^2\rangle$, (au)^2) for the Excited States of CH_2N_2 at EOM-CCSD/6-311(3+,+)G*[a]

state	ΔE_{vert}	f_L	μ^2_{tr}	$\Delta\langle Y^2\rangle$	$\Delta\langle X^2\rangle$	$\Delta\langle Z^2\rangle$
$1^1A_2(\pi^*_\sigma \leftarrow \pi)$	3.21	0	0	1	−2	1
$1^1B_1(3s \leftarrow \pi)$	5.33	0.0200	0.1186	15	10	6
$2^1A_1(\pi^* \leftarrow \pi)$	5.85	0.2100	1.4904	5	16	14
$2^1A_2(3p_y \leftarrow \pi)$	6.35	0	0	39	10	7
$2^1B_1(3p_z \leftarrow \pi)$	6.39	0.0100	0.0644	13	11	41
$3^1B_1(3d^2_z \leftarrow \pi)$	7.08	0.0100	0.0431	24	22	74
$3^1A_1(3p_x \leftarrow \pi)$	7.15	0.0700	0.3821	23	69	16
$3^1A_2(3d_{yz} \leftarrow \pi)$	7.23	0	0	53	15	48
$4^1B_1(4s \leftarrow \pi)$	7.34	0.0010	0.0071	75	76	33
$4^1A_1(3d_{xz} \leftarrow \pi)$	7.36	0.0001	0.0005	22	68	63
$5^1A_1(4p_x \leftarrow \pi)$	7.77	0.0100	0.0582	69	210	82

[a] At the B3LYP/6-311G(2df,p) optimized geometry; E_{CCSD}= −148.426979 hatree.

In the second set of experiments, CH_2N_2 was again ionized by 2 + 1 REMPI and images of the ejected photoelectrons were obtained at selected wavelengths in the 51 000−58 900 cm^{-1} (6.32−7.30 eV) region. Using the velocity map imaging technique,[19] event counting and centroiding,[20,21] and the basis set expansion (BASEX) Abel transform method,[22] photoelectron kinetic energy (eKE) distributions were determined from the images. Electrons produced in the ionization chamber were extracted and accelerated by the ion optics into the TOF mass spectrometer and detected with the same MCP detector. Signals from the detector were monitored with a CCD camera (Imager 3, 12 bit, LaVision, 640 × 480 pixel array) and transferred to a PC for analysis.

3. Computational Details

The equilibrium geometry and vibrational frequencies of neutral CH_2N_2 were calculated by CCSD(T),[23,24] using the cc-pVTZ basis,[25] and by B3LYP,[26] using the 6-311G(2df,p) basis. Geometry and frequencies of the ground state of the cation were calculated by CCSD(T)/cc-pVTZ, using the unrestricted (UHF) reference. Vertical excitation energies from the ground state were calculated using EOM-CCSD[27,28]/6-311(3+,+)G* at the B3LYP optimized geometry. The basis sets were derived from the polarized split-valence 6-311G(d,p) basis by adding additional polarization and diffuse functions.[29,30]

The error bars[31] for equilibrium geometries for CCSD(T)/cc-pVTZ are much lower than the geometrical changes observed in this study. Nonsystematic errors for bond lengths are on the

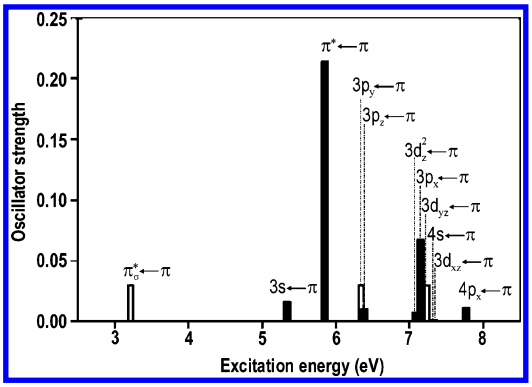

Figure 3. Bars showing calculated vertical excitation energies of CH_2N_2. Allowed and forbidden transitions are indicated by filled and hollow bars, respectively.

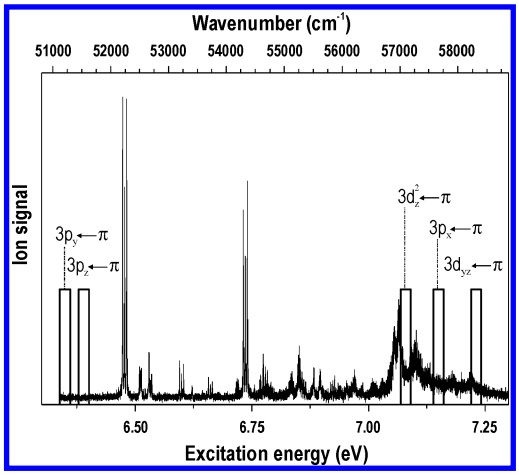

Figure 4. Survey 2 + 1 REMPI spectrum in the 6.32−7.30 eV (51 000−58 900 cm^{-1}) region. The empty bars indicate the calculated values of vertical excitation energies.

order of about 0.002 Å. CCSD(T) underestimates bond angles by about 0.5° and has a nonsystematic error of about 1°. EOM-CCSD excitation energies are accurate to within 0.1−0.3 eV.[32] A basis set with adequate diffuse functions is necessary for states with Rydberg character.

As in our previous work,[33] the assignment of valence and Rydberg character to the excited states was based on: (i) the symmetry of the transition, (ii) leading EOM-CCSD amplitudes and the character of the corresponding HF orbitals, and (iii) the second moments $\langle X^2\rangle$, $\langle Y^2\rangle$, and $\langle Z^2\rangle$ of the EOM-CCSD electron density. The character of the HF orbitals was determined using the Molden interface.[34] All optimizations, frequencies, and excited state calculations were performed using the Q-Chem[35] and ACES II[36] electronic structure programs. Franck−Condon factors were modeled using the PES4 program.[37]

4. Computational Results

a. Equilibrium Geometries and Ionization Energies. The equilibrium geometries of neutral diazomethane in its ground (1^1A_1) and Rydberg 3p excited states, as well as of the cation in its ground (1^2B_1) state, are shown in Figure 2. Both the CCSD(T) and B3LYP optimized geometries agree with experimentally determined values,[38] which are also summarized in this figure. The first ionization removes an electron from the highest occupied, out-of-plane π orbital (Figure 1) with vertical IE of 8.95 eV, as calculated by EOM-IP-CCSD[39−41] with 6-311G(2df,p) basis set. The experimental vertical IE is 9.00 eV,[6] and the adiabatic IE calculated at CCSD(T)/cc-pVTZ geometries and corrected by zero point energy is 8.84 eV. The second ionization energy, which corresponds to removing an electron from the π^*_σ orbital (Figure 1) in the plane of the molecule, is much higher and equals 14.00 eV vertically at the EOM-IP−CCSD level. Calculated structural changes resulting from the first ionization are consistent with removing an electron from a bonding π orbital. The CN bond length increases substantially (by 0.064 Å) due to a decrease in bond order. At the same time, the NN bond length slightly contracts (by 0.024 Å) due to the antibonding nature of the π orbital along the NN bond. The increase in HCH angle relative to the neutral (by 2.8°) is due to depleted electron density along the CN bond, which allows the two CH bonds to move away from each other to minimize electrostatic repulsion. The molecule has C_{2v} symmetry in both the neutral and the cation ground states.

b. Excited Electronic States. The vertical excitation energies, oscillator strengths, transition dipole moments, and second moments of the excited states of CH_2N_2 are listed in Table 1. The excitation energies and oscillator strengths are also plotted as a stick spectrum in Figure 3. In the C_{2v} point group, states of A_2 symmetry have zero oscillator strength in one-photon excitation; these are depicted by hollow bars. The electronic spectrum is fairly dense in the 5.00 − 8.00 eV region and dominated by Rydberg transitions. All of the calculated singlet states derive from excitations from the highest occupied π orbital.

TABLE 2: Calculated Vertical (ΔE_{vert}) and Adiabatic (ΔE_{ad}) Excitation Energies and Quantum Defects (δ) and the Corresponding Experimental Values

state	ΔE_{vert}	ΔE_{ad}	$\Delta E_{vert-ad}$	E_{exp}	δ_{calcd}	δ_{exp}
$2^1A_2(3p_y \leftarrow \pi)$	6.35	6.24	0.11	6.48[a]	0.73	0.68
$2^1B_1(3p_z \leftarrow \pi)$	6.39	6.30	0.09	6.52[b]	0.72	0.66
$3^1A_1(3p_x \leftarrow \pi)$	7.15	6.91	0.24	7.05[c]	0.29	0.36
$1^2B_1(\infty \leftarrow \pi)$	8.95	8.85	0.10	9.00[d]		

[a] Measured at 52 227 cm^{-1} ($K' = 0 \leftarrow K'' = 0$ and $K' = 1 \leftarrow K'' = 1$). [b] Measured at 52 679 cm^{-1} ($K' = 0 \leftarrow K'' = 1$). [c] Measured at 56 898 cm^{-1}. [d] Ref 6.

The lowest singlet excited state, which is well separated from the others and lies at 3.21 eV, corresponds to the valence $1^1A_2 \leftarrow 1^1A_1$ ($\pi_\sigma^* \leftarrow \pi$) transition. In one-photon absorption, this state was observed as a weak, broad band centered at 3.14 eV. This one-photon forbidden transition becomes weakly allowed by vibronic couplings with other electronic states.

In the 5.00−6.00 eV region, we found two transitions: the Rydberg $1^1B_1 \leftarrow 1^1A_1$ ($3s \leftarrow \pi$) transition at 5.33 eV, and the valence transition $2^1A_1 \leftarrow 1^1A_1$ ($\pi^* \leftarrow \pi$) at 5.85 eV. In agreement with the antibonding valence character of the upper state, the latter transition has oscillator strength an order of magnitude higher than the Rydberg's (oscillator strength 0.21 compared to 0.02) due to high spatial overlap between the π and π^* orbitals. In this region (5.50−7.00 eV), Rabalais assigned a single intense, broad band centered at 5.70 eV based on known data,[42] but diffuse structures have also been reported.[10,11] The neighboring Rydberg state is likely hidden under the intense valence band.

Between 6.00 and 7.00 eV, our calculations predict only two electronic transitions: the $2^1A_2 \leftarrow 1^1A_1$ ($3p_y \leftarrow \pi$) and $2^1B_1 \leftarrow 1^1A_1$ ($3p_z \leftarrow \pi$) at vertical excitation energies 6.34 and 6.38 eV, respectively. In the region 7.00−7.25 eV, three electronic transitions have been calculated (Table 1): $3^1B_1 \leftarrow 1^1A_1$ ($3d^2_z \leftarrow \pi$) (vertical excitation energy 7.08 eV), $3^1A_1 \leftarrow 1^1A_1$ ($3p_x \leftarrow \pi$) (7.15 eV), and $3^1A_2 \leftarrow 1^1A_1$ ($3d_{yz} \leftarrow \pi$) (7.23 eV). The

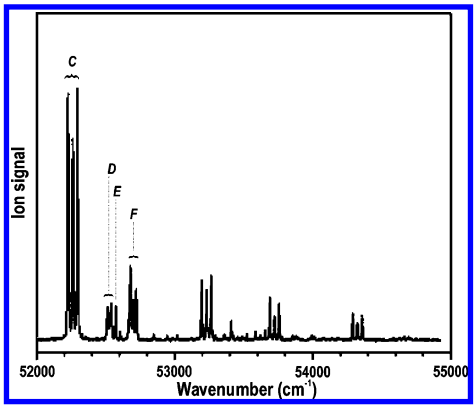

Figure 5. 2 + 1 REMPI spectrum of diazomethane in the region of excitations to the $^1A_2(3p_y)$ and $^1B_1(3p_z)$ states obtained by measuring $m/e = 42$ as a function of excitation energy. The laser wavelength increment was 0.005 nm. See the text for details of the C−F bands.

latter has zero oscillator strength due to symmetry and could only borrow intensity. The $3^1B_1 \leftarrow 1^1A_1$ ($3d^2_z \leftarrow \pi$) transition has very low oscillator strength; also, its pure Rydberg character does not imply any broadening. The calculated vertical excitation energies, superimposed on the 2 + 1 REMPI spectrum, are shown in Figure 4.

The $3^1A_1 \leftarrow 1^1A_1$ ($3p_x \leftarrow \pi$) Rydberg transition has oscillator strength about one order of magnitude greater than transitions to the other 3p states due to mixing with the valence $1^1A_2 \leftarrow 1^1A_1$ ($\pi^* \leftarrow \pi$) transition of the same symmetry. This is confirmed by the composition of its EOM-CCSD wavefunction, which contains a large contribution from the $\pi^* \leftarrow \pi$ configuration. Both the intensity and diffuse nature of the two peaks observed in the 56 860−58 900 cm^{-1} region (see below) suggest assignment of this band as the $3^1A_1 \leftarrow 1^1A_1$ ($3p_x \leftarrow \pi$) Rydberg transition.

The vertical and adiabatic excitation energies for the Rydberg 3p states and the cation ground state (1^2B_1) are compared with the experimental result in Table 2. The $3^1A_1 \leftarrow 1^1A_1$ ($3p_x \leftarrow \pi$) transition shows the largest difference between its vertical and adiabatic excitation energies (0.24 eV), whereas the $2^1A_2 \leftarrow 1^1A_1$ ($3p_y \leftarrow \pi$) and $2^1B_1 \leftarrow 1^1A_1$ ($3p_z \leftarrow \pi$) transitions exhibit much smaller differences (∼0.1 eV) and are within 0.02 eV of each other. The magnitude of the vertical-adiabatic relaxation in these states is close to that in the cation, supporting their description as pure, cation-like Rydberg states. The $3^1A_1 \leftarrow 1^1A_1$ ($3p_x \leftarrow \pi$) transition's large difference indicates strong Rydberg/valence mixing.

Referring to the equilibrium geometries of the states shown in Figure 2, we find that the $2^1A_2(3p_y)$ and $2^1B_1(3p_z)$ states are more similar in structure to the 1^2B_1 cation than to the neutral. The $3^1A_1(3p_x)$ state, in contrast, is different than both the cation and the other two 3p states. Whereas the 1^2B_1 cation and the 2^1A_2 and 2^1B_1 neutral excited states retain the C_{2v} symmetry of the neutral ground state, the $3^1A_1(3p_x \leftarrow \pi)$ state has C_s equilibrium structure. The CN bond length increases and the CNN bond is no longer linear (161°, Figure 2). The plane of the CH_2 sp^2 center is also broken by about 3°. This twisted geometry reflects the partial population of the strongly antibonding π^* orbital.

The $3p_y$ and $3p_z$ orbitals in diazomethane are oriented to maximize overlap with the positive centers of the nuclear charge distribution. According to natural bond order (NBO) analysis,[43] about half of the +1 charge of the nuclear core is accommodated by the hydrogens. The lobes of the $3p_y$ orbital have highest

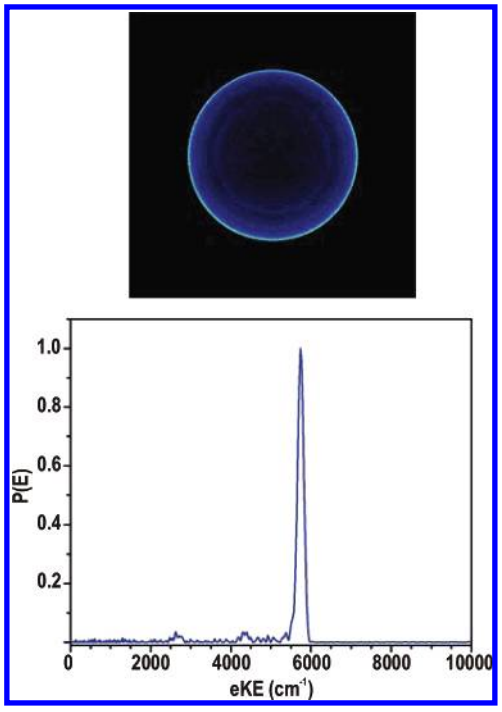

Figure 6. Photoelectron image and the corresponding eKE distributions obtained at excitation wavelength $\lambda = 382.69$ nm ($2h\nu = 52\,262$ cm^{-1}; middle peak of band C).

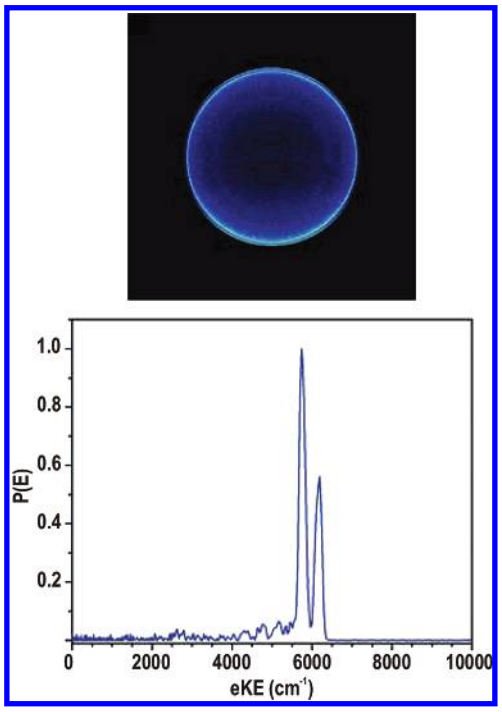

Figure 7. Photoelectron image and the corresponding eKE distributions obtained at excitation wavelength 380.75 nm (52 528 cm^{-1}; middle peak of band D).

density on top of the hydrogen atoms (Figure 1). Donation into the electron-deficient CH bonds leads to a contracted CH bond length relative to the cation and a larger HCH bond angle (Figure 2). A similar effect along the CNN bonds is prevented by symmetry.

In contrast, the $3p_z$ orbital has significant density along the CNN axis. The resulting electronic donation leads to contracted CN and NN bond lengths relative to the cation and a smaller

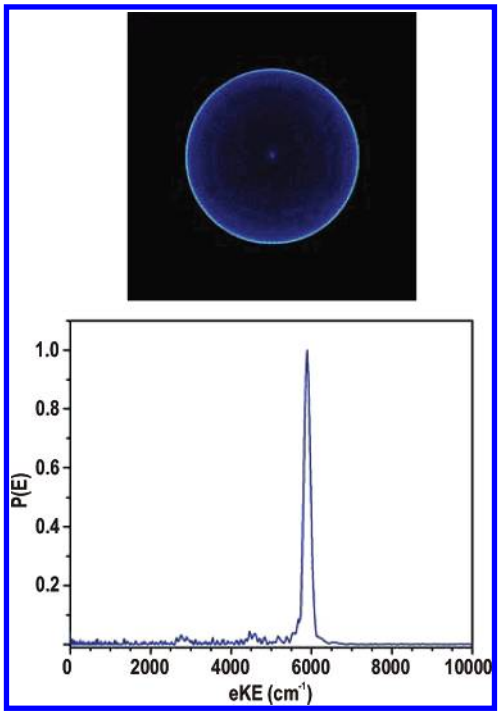

Figure 8. Photoelectron image and the corresponding eKE distributions obtained at excitation wavelength 380.39 nm (52 577 cm^{-1}; band E).

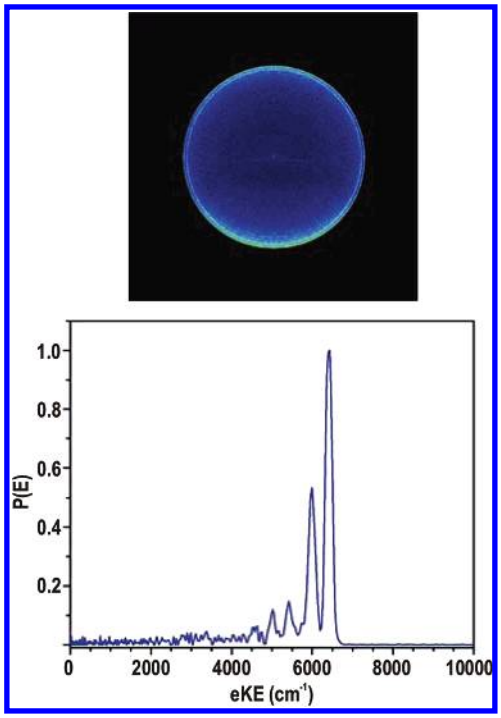

Figure 9. Photoelectron image and the corresponding eKE distributions obtained at excitation wavelength 379.50 nm (52 700 cm^{-1}; middle peak of band F).

HCH angle to minimize electrostatic repulsion. Similar effects have been seen in the electronic structure of several vinyl radicals.[33]

5. Experimental Results

The 2 + 1 REMPI spectrum of CH_2N_2 recorded by monitoring the parent mass peak (m/e = 42) as a function of laser excitation at 51 000−58 900 cm^{-1} (6.32−7.30 eV) is shown in Figure 4, whereas Figure 5 shows an expanded region (52 000−55 000 cm^{-1}; 6.45−6.82 eV) recorded at higher resolution (smaller step size). The dependence of the parent ion signal on laser pulse energy, determined at several excitation wavelengths, is nearly quadratic. This suggests that the observed spectral features derive from two-photon resonances. The laser frequency was calibrated to published lines of diazomethane in the region ~52 512−52 721 cm^{-1}.[12]

To characterize the C−F bands near the observed onset of the absorption in this region, photoelectron kinetic energy (eKE) distributions were obtained by imaging following ionization of selected levels of the excited state(s). Figures 6−9 show photoelectron images obtained at excitation wavelengths λ = 382.69 nm ($2h\nu$ = 52 262 cm^{-1}; middle peak of band C), 380.75 nm (52 528 cm^{-1}; middle peak of band D), 380.39 nm (52 577 cm^{-1}; band E), and 379.50 nm (52 700 cm^{-1}; middle peak of band F), respectively, and the corresponding eKE distributions. In all images, the electric field vector of the laser is set parallel to the vertical direction of the image plane. The relative width of the peaks is $\Delta E/E$ = 3.0 ± 0.2%, limited by instrument resolution. There is one strong, narrow band in each of the eKE distributions obtained at λ = 382.69 nm (at 5742 cm^{-1}; Figure 6) and λ = 380.39 nm (at 5889 cm^{-1}; Figure 8). Both photoelectron images have an isotropic angular distribution. The eKE distributions obtained at λ = 380.75 nm (52 528 cm^{-1}) and at 379.50 nm (52 700 cm^{-1}) are also similar to each other (Figures 7 and 9) but different from those shown in Figures 6 and 8. First, each has two strong narrow bands (at 5754 and 6172 cm^{-1} in Figure 7 and 5994 and 6414 cm^{-1} in Figure 9), and in each, the two peaks are separated by ~420 ± 20 cm^{-1}. Second, both distributions exhibit a weak progression of three peaks with ~400 ± 20 cm^{-1} separation. Last, the strong outermost ring in both images has an anisotropic angular distribution, whereas the strong inner rings are isotropic. It is difficult to characterize the angular distributions of the photoelectrons corresponding to peaks of the weak vibrational

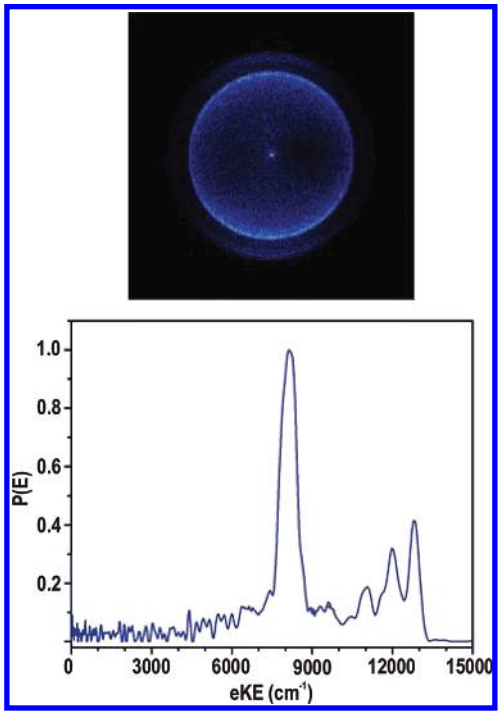

Figure 10. Photoelectron image and the corresponding eKE distributions obtained at excitation wavelength λ = 351.09 nm (56 965 cm^{-1}).

progression because of their low intensities. The main difference between the two eKE distributions shown in Figures 7 and 9 is in the relative intensities of the two intense features.

The band at ~7.05−7.30 eV (~56 860−58 900 cm^{-1}) shown in Figure 4 is much more diffuse than the other bands in this region. Figure 10 shows a photoelectron image and the corresponding photoelectron KE distribution obtained at $\lambda = 351.09$ nm (56 965 cm^{-1}). It has an intense band at 8098 cm^{-1}, as well as a progression of three peaks at 11 020, 11 992, and 12 800 cm^{-1}, and is very different from the distributions shown in Figures 6−9. The relative width of the peaks $\Delta E/E = 8.7 \pm 0.2\%$, is broader than the instrumental resolution.

6. Discussion

Promotion of an electron from the highest occupied π molecular orbital of CH_2N_2 (Figure 1) into 3p atomic-like orbitals generates the $3^1A_1(3p_x \leftarrow \pi)$, $2^1A_2(3p_y \leftarrow \pi)$, and $2^1B_1(3p_z \leftarrow \pi)$ Rydberg states. These states correlate with the ground state of the ion, $1^2B_1(\infty \leftarrow \pi)$. For small molecules, the excitation energies of the Rydberg states can often be approximated by the Rydberg formula:[8]

$$E_{\mathrm{Ryd}} = \mathrm{IE} - 109\,737.3/(n-\delta)^2\ \mathrm{cm}^{-1} \qquad (1)$$

where E_{Ryd} is the excitation energy of the Rydberg state (in cm^{-1}), IE is the adiabatic ionization energy (in cm^{-1}), n is the principal quantum number, and δ is the quantum defect. The calculated and experimental quantum defects are listed in Table 2. Typical values for $n = 3$ Rydberg states are ~0.9−1.2, 0.4−0.7, and ~0.1 for s, p, and d states, respectively. The calculated and experimental quantum defects for the $3^1A_1(3p_x)$ state fall outside this region and differ from the values for the other two Rydberg states, in agreement with its partial valence composition. Below we discuss first the $2^1A_2(3p_y \leftarrow \pi)$ and $2^1B_1(3p_z \leftarrow \pi)$ Rydberg states, followed by a discussion of the $3^1A_1(3p_x \leftarrow \pi)$ state.

a. The $2^1A_2(3p_y \leftarrow \pi)$ and $2^1B_1(3p_z \leftarrow \pi)$ Rydberg States and their Interaction. The internal energy (E_{int}) of the ion corresponding to each measured photoelectron peak is obtained from the peak position of the eKE distribution:

$$E_{\mathrm{int}} = 3h\nu - \mathrm{eKE} - \mathrm{IE} \qquad (2)$$

In the 2 + 1 REMPI spectrum of CH_2N_2 shown in Figure 5, the first group of three peaks (band C; 52 227−52 295 cm^{-1}) was not observed in the one-photon absorption spectrum reported by Merer. We assign this group to the origin band of the $2^1A_2 \leftarrow 1^1A_1$ transition for the following reasons. According to electric−dipole transition selection rules in C_{2v} symmetry, the $A_2 \leftarrow A_1$ transition is optically forbidden in one-photon but allowed in two-photon excitation. The onset of this transition is close to the calculated one, and its quantum defect ($\delta = 0.68$) is typical of a Rydberg p state. The Rydberg nature of the state is also confirmed by the photoelectron image (Figure 6) obtained at $\lambda = 382.69$ nm (52 262 cm^{-1}). From the correpsonding eKE distribution shown in Figure 6, we conclude that the $CH_2N_2^+$ ions are generated in the vibrational ground state. This suggests a similarity in geometries of the neutral excited state and ion ground state, which results in a propensity for ionization via the diagonal $1^2B_1 \leftarrow 2^1A_2$ $(\infty \leftarrow 3p_y)$ 0_0^0 transition. The internal energy of the ion obtained by excitation through the 0_0^0 band is ~60 cm^{-1}, indicating little rotational excitation in the neutral parent. Similar photoelectron kinetic energy distributions are obtained for the other two peaks in this triad.

Additional support for this assignment is obtained from the ab initio calculations, which show the presence of only two electronic states in this region (Table 1): the $2^1A_2(3p_y \leftarrow \pi)$ state at 6.34 eV (51 213 cm^{-1}) and the $2^1B_1(3p_z \leftarrow \pi)$ state at 6.38 eV (51 535 cm^{-1}). The $^1B_1 \leftarrow {}^1A_1$ transition is optically allowed in one-photon excitation but the $^1A_2 \leftarrow {}^1A_1$ is not, and therefore the observed band located at 52 227−52 295 cm^{-1}, which has not been seen in one-photon absorption, is assigned as the band origin of $2^1A_2 \leftarrow 1^1A_1$ $(3p_y \leftarrow \pi)$ transition.

The three components of the band are attributed to resolved K structure. CH_2N_2 in its neutral ground state (1^1A_1) is a near-symmetric prolate top ($A'' = 9.112$ cm^{-1}, $B'' = 0.377$ cm^{-1}, and $C'' = 0.362$ cm^{-1}),[8] and according to calculations, its 3p Rydberg states also have C_{2v} symmetry (except $3^1A_1(3p_x)$). In C_{2v}, transitions to the vibronic bands of A_1 and A_2 symmetry are expected to be governed by $\Delta K = 0, \pm 2$ selection rules with a $4A''$ spacing between K bands.[44] Transitions to B_1 and B_2 vibronic bands are governed by $\Delta K = \pm 1$ selection rules, with a $2A''$ spacing. The separation of ~35 cm^{-1} between the three peaks in this groups, which is approximately equal to $4A''$, indicates that the rotational transition is governed by $\Delta K = 0, \pm 2$ selection rules and that the excited state is of A symmetry. All of the observed transitions originate in $K = 0$ and 1, the only ones significantly populated in the supersonic expansion. The first peak, in order of increasing energy, arises from the $K' = 0 \leftarrow K'' = 0$ and $K' = 1 \leftarrow K'' = 1$ transitions. The next two components of this triad correspond to the $K' = 2 \leftarrow K' = 0$ and $K' = 3 \leftarrow K'' = 1$ transitions, respectively. In this triad, the outermost bands are more intense because they include transitions from $K'' = 1$, which according to nuclear-spin statistics are ×3 more intense than those from $K'' = 0$.

The next three groups of bands at 52 513−52 541 cm^{-1}, 52 574 cm^{-1}, and 52 679−52 722 cm^{-1} were observed in one-photon absorption and assigned by Merer as transitions to three different electronic states denoted as $D(^1B_1)$, $E(^1B_2)$, and $F(^1B_1)$, respectively. According to the ab initio calculations, there exist only two electronic states ($2^1B_1(3p_z)$ and $2^1A_2(3p_y)$) in this energy region. The absence of other states within the error bars of the method make this assignment conclusive.

The photoelectron spectra can aid in assigning the spectra. The bands with partially resolved rotational structure at 52 513−52 541 cm^{-1} (D) and 52 679−52 722 cm^{-1} (F) are assigned as mixed bands composed of the 9_0^1 transition to the $2^1A_2(3p_y)$ state and the band origin of the $2^1B_1(3p_z) \leftarrow 1^1A_1$ transition. This assignment is based on the two-peak structure in the eKE distributions shown in Figures 7 and 9. Comparing the two eKE distributions, which have equal energy separations but different peak heights, suggests that two electronic states are coupled. The difference in anisotropy of the strong inner and outer rings also suggests that the photoelectrons corresponding to these rings may be ejected from different electronic states. In Merer's absorption experiments, the optically forbidden 9_0^1 band of the $2^1A_2(3p_y) \leftarrow 1^1A_1$ transition becomes allowed by vibronic coupling to the $2^1B_1(3p_z)$ state mediated by the nontotally symmetric ν_9' (b_2) vibration. B_1 symmetry in the 2^1A_2 state is obtained for A_2(electronic symmetry) × b_2(vibrational symmetry) vibronic bands.

Because the eKE distributions in Figures 7 and 9 display only two major peaks, we use a two state approximation to obtain the energy of the deperturbed states and the coupling matrix

TABLE 3: CCSD(T)/cc-pVTZ Harmonic Vibrational Frequencies for Cation Ground State (1^2B_1)

mode	assignment	symmetry	frequency, cm^{-1}
ν_1^+	CH_2 symmetric stretching	a_1	3164
ν_2^+	NN stretching	a_1	2199
ν_3^+	CH_2 symmetric bending	a_1	1432
ν_4^+	CN stretching	a_1	1001
ν_5^+	CNN bending (out-of-plane)	b_1	440
ν_6^+	CH_2 wagging	b_1	712
ν_7^+	CH_2 asymmetric stretching	b_2	3311
ν_8^+	CH_2 rocking	b_2	1133
ν_9^+	CNN bending (in-plane)	b_2	377

elements. The two molecular eigenstates $|\psi_-\rangle$ and $|\psi_+\rangle$ are expressed as linear combinations:

$$|\psi_-\rangle = -\beta|\phi_1\{0_0^0(a_1), {}^1B_1(3p_z)\}\rangle + \alpha|\phi_2\{9_0^1(b_2), {}^1A_2(3p_y)\}\rangle \quad (3)$$

$$|\psi_+\rangle = \alpha|\phi_1\{0_0^0(a_1), {}^1B_1(3p_z)\}\rangle + \beta|\phi_2\{9_0^1(b_2), {}^1A_2(3p_y)\}\rangle \quad (4)$$

We obtain $|\alpha^2|$ and $|\beta^2|$ from the relative peak heights in the two photoelectron distributions, giving an average ratio of $|\alpha|^2/|\beta|^2 = 1.82$. Using $|\alpha^2| + |\beta^2| = 1$, we obtain $\alpha = 0.8$ and $\beta = 0.6$, and putting these values into the two-state coupled equations (see Appendix), we finally obtain: $E_1 = 52\,638\ cm^{-1}$, $E_2 = 52\,590\ cm^{-1}$, and $V_{12} \sim 83\ cm^{-1}$, where $E_{1,2}$ are the deperturbed energies of the two states and V_{12} is the coupling matrix element. The eKE distributions show that the F band ($52\,679-52\,722\ cm^{-1}$) has a larger contribution from the 2^1B_1-($3p_z$) state, and therefore $E_1 = 52\,638\ cm^{-1}$ is assigned as the adiabatic origin of this state. Its associated quantum defect, $\delta = 0.65$, is typical of a Rydberg p state.

The peaks in the eKE distributions shown in Figures 7 and 9 correspond to vibrational levels ν_0^+, ν_9^+, and $\nu_4^+ + n\nu_9^+$ ($n = 0-2$) in the $CH_2N_2^+$ ion (where ν_9^+ is the CNN in-plane bend and ν_4^+ is the CN stretch). The frequency of $\nu_9{}^+$ is $\sim 420 \pm 10\ cm^{-1}$, and the frequencies of $\nu_4{}^+ + n\nu_9^+$ combination modes are $1002 \pm 20\ cm^{-1}$, $1404 \pm 30\ cm^{-1}$, and $1808 \pm 40\ cm^{-1}$ for $n = 0$, 1, and 2, respectively. The existence of a vibrational progression suggests that there is a small geometry change between the Rydberg and the cation states. Calculated vibrational frequencies for the ground state of the 1^2B_2 cation are given in Table 3 for comparison. The ν_4^+ fundamental band was observed before in the He I PES with a frequency of $970 \pm 80\ cm^{-1}$.[6]

The three K bands of each of the mixed transitions of B_1 symmetry are separated by ~ 14 and $\sim 21\ cm^{-1}$ (approximately $2A''$). This indicates that these transitions are governed by $\Delta K = \pm 1$ selection rules and confirms that the excited states have B symmetry. The contributions to the three components, in order of increasing energy, are from the $K' = 0 \leftarrow K'' = 1$, $K' = 1 \leftarrow K'' = 0$, and $K' = 2 \leftarrow K'' = 1$ transitions.

The band at $52\,574\ cm^{-1}$ [E($^1B_2$), Figure 8] is assigned as the 5_0^1 transition to $2^1A_2(3p_y)$. The single peak in the corresponding eKE is assigned as ν_5^+ (b_1; CNN out-of-plane bend) of $CH_2N_2^+$ whose frequency is $318 \pm 10\ cm^{-1}$. The slight difference between the value reported here and that given by Merer[12] ($52\,598.7\ cm^{-1}$ and $52\,668.6\ cm^{-1}$ for the $K' = 2 \leftarrow K'' = 3$, and $K' = 2 \leftarrow K'' = 1$ transitions, respectively) reflects the lower rotational temperature in our experiment, where only $K'' = 0$, 1 are significantly populated.

All of the other bands in the region $52\,000-55\,000\ cm^{-1}$ are fairly sharp and have a typical triad K structure. Their photoelectron spectra display single peaks, and they are assigned to unperturbed transitions to the $2^1A_2(3p_y \leftarrow \pi)$ state. A detailed analysis of the vibronic spectrum will be given in a separate publication. Here we note only that, from the widths of the bands, we conclude that the $2^1A_2(3p_y \leftarrow \pi)$ state is bound and only weakly predissociative.

Finally, we compare briefly our interpretation of the coupled states to the one offered by Merer. As discussed above, we see evidence only for coupling of two bands, D and F, of B_1 vibronic symmetry, and no evidence for coupling in the E($^1B_2$) band. In contrast, Merer concluded that all three bands interact via Coriolis coupling. This conclusion was reached in analogy with the interaction of the ν_5'', ν_6'', and ν_9'' vibrational modes of the neutral ground state of diazomethane **(**1^1A_1),[45] which couple the b_2 level via Coriolis interaction with two b_1 levels. The difference may derive from the rotational excitation of the parent. Merer carried out his measurements at 300 and 196 K, where K' levels up to $K' = 10$ are populated, whereas in our molecular beam measurements ($T_{rot} \sim 10$ K), only $K' \leq 2$ are significantly populated. Using the Coriolis constants given by Merer, we obtain the values of the $|V_{FE}|$ and $|V_{ED}|$ Coriolis coupling matrix elements for $K' = 10$ are ~ 82 and $\sim 142\ cm^{-1}$, respectively, whereas for $K' = 2$, the corresponding terms are 5 times smaller (~ 16 and $\sim 28\ cm^{-1}$, respectively). The direct coupling matrix element between the F and D state obtained in our study, $|V_{FD}| \sim 83\ cm^{-1}$, is much higher than the $|V_{FE}|$ and $|V_{ED}|$ Coriolis coupling matrix elements for $K' = 2$. These considerations and the photoelectron images support our interpretation that, at low rotational temperatures, there is significant interaction only between the two states of $^1B_1$ symmetry.

b. The $3^1A_1(3p_x \leftarrow \pi)$ State. In the $57\,000\ cm^{-1}$ region of the one-photon absorption spectrum, two strong diffuse bands spaced by $\sim 430 \pm 20\ cm^{-1}$ were observed by Merer.[12] These bands did not fit the previous progressions, and it was suggested that they represent more than one electronic state.

As discussed above, our EOM-CCSD study of the excited states of CH_2N_2 using the 6-311(3+,+)G* basis set reveals several states in this region (Figure 4): $3^1B_1(3d^2{}_z \leftarrow \pi)$, 3^1A_1-($3p_x \leftarrow \pi$), and $3^1A_2(3d_{yz} \leftarrow \pi)$). The latter cannot be observed in one-photon absorption due to symmetry considerations. The $3^1B_1(3d^2{}_z \leftarrow \pi)$ state has very low oscillator strength, and its pure Rydberg character should not result in the significant broadening observed in the measurements. The transition to the $^1A_1(3p_x)$ state has the largest oscillator strength among the Rydberg states in this region due to its mixing with the valence $2^1A_1(\pi^* \leftarrow \pi)$ state. Therefore the $3^1A_1 \leftarrow 1^1A_1$ ($3p_x \leftarrow \pi$) transition is the best candidate for these bands. Calculations of the geometries of the excited states show that the geometry of the $3^1A_1(3p_x)$ state differs considerably from that of 2^1A_2-($3p_y \leftarrow \pi$), $2^1B_1(3p_z \leftarrow \pi)$, and the cation $1^2B_1(\infty \leftarrow \pi)$. The $3^1A_1(3p_x \leftarrow \pi)$ state has an in-plane bent geometry corresponding to C_s symmetry, as discussed in Section 4b.

The different geometries of the neutral $3^1A_1(3p_x)$ and the cation 1^2B_1 states should give rise to a propensity for ionization via off-diagonal transitions, resulting in multiple peaks in the photoelectron spectrum as indeed seen in the experiment. The eKE distribution obtained at $\lambda = 351.09$ nm ($56\,965\ cm^{-1}$) has an intense band at $8098\ cm^{-1}$, and a progression of three peaks at 11 020, 11 992, and $12\,800\ cm^{-1}$ (Figure 10). This progression can be assigned to excitation of the ν_6^+ (CH_2 wag**)** mode in the cation. The experimental frequencies for ν_6^+ and $2\ \nu_6^+$ are 808 ± 30 and $1780 \pm 70\ cm^{-1}$, respectively, suggesting that these modes are rather anharmonic. The theoretical harmonic

frequency for the ν_6^+ mode is 712 ± 20 cm^{-1}. The strong peak at 8089 cm^{-1} can be assigned to excitation of either $\nu_1^+ + \nu_3^+$ or $\nu_7^+ + \nu_3^+$ vibrations (4765 ± 190 cm^{-1}) in the cation (where ν_1^+ and ν_3^+ are the CH_2 symmetric stretch and bend, respectively, and ν_7^+ is the CH_2 asymmetric stretch). The eKE distributions at $\lambda = 351.51$ nm (56 898 cm^{-1}) and $\lambda = 349.28$ nm (57 261 cm^{-1}) have similar character. The diffuse nature of the bands is attributed to their strong coupling to the 2^1A_1-($\pi^* \leftarrow \pi$) valence state, which lends them oscillator strength and is repulsive. The observed dissociation products, $N_2(^1\Sigma_g^+)$ + $CH_2(\tilde{c}^1A_1)$, indeed correlate with a molecular state of A_1 symmetry.

7. Conclusions

The electronic states of diazomethane in the region 3.00−8.00 eV have been obtained by ab initio calculations, and transitions in the region 6.32−7.30 eV have been characterized experimentally using a combination of 2 + 1 REMPI spectroscopy and photoelectron imaging in a molecular beam. Specifically, in the region where experiments have been carried out, we find that only three Rydberg 3p states are excited, the 2^1A_2-($3p_y \leftarrow \pi$), $2^1B_1(3p_z \leftarrow \pi)$, and $3^1A_1(3p_x \leftarrow \pi)$. The former two states are of mostly pure Rydberg character, whereas the 3^1A_1-($3p_x \leftarrow \pi$) state is mixed with the valence $2^1A_1(\pi^* \leftarrow \pi)$ state and is strongly predissociative. We find that the ground vibrational level of the $2^1B_1(3p_z)$ state is mixed with the 2^1A_2-($3p_y$) ν_9 level, which is of B_1 vibronic symmetry. The other $2^1A_2(3p_y)$ vibronic states exhibit pure Rydberg character and generate ions in single vibrational states. They also predissociate rather slowly. Thus, this state can serve both as a sensitive and state-specific two-photon diagnostic for diazomethane and as a gateway state for preparation of diazomethane ions in specific vibrational levels. The photoelectron spectra of the $3^1A_1(3p_x \leftarrow \pi)$ state, on the other hand, give rise to many states of the ion. The two-photon excitation scheme used here excited efficiently vibronic levels in the $2^1A_2(3p_y)$ state, whereas vibronic levels of the $2^1B_1(3p_z)$ state are best reached by one-photon absorption, as done by Merer.[12]

The experimental and theoretical results agree very well both in regard to excitation energies and to vibrational modes of the ion. Analysis of the photoelectron spectra of the excited states elucidates the interactions between the Rydberg electron with the ion core and reveals mixings with valence states.

Acknowledgment. We thank Karl O. Christe and C. J. Bigler Jones for their generous help in the modification of the CH_2N_2 synthesis procedure for molecular beam conditions. This work was carried out in the framework of the Center for Computational Studies of Electronic Structure and Spectroscopy of Open-Shell and Electronically Excited Species supported by the National Science Foundation through the CRIF:CRF CHE-0625419, CHE-0624602, and CHE-0625237. Support of this work by Chemical Sciences, Geosciences and Biosciences Division, Office of Basic Energy Sciences, U.S. Department of Energy is gratefully acknowledged.

Appendix

The wave functions $|\psi_-\rangle$ and $|\psi_+\rangle$ of the perturbed states are represented as linear combinations of the wave functions $|\phi_1\{0_0^0(a_1),{}^1B_1(3p_z)\}\rangle$ and $|\phi_2\{9_0^1(b_2),{}^1A_2(3p_y)\}\rangle$ of the unperturbed states:

$$|\psi_-\rangle = -\beta|\phi_1\{0_0^0(a_1),\,{}^1B_1(3p_z)\}\rangle + \alpha|\phi_2\{9_0^1(b_2),\,{}^1A_2(3p_y)\}\rangle \quad \text{(A1)}$$

$$|\psi_+\rangle = \alpha|\phi_1\{0_0^0(a_1),\,{}^1B_1(3p_z)\}\rangle + \beta|\phi_2\{9_0^1(b_2),\,{}^1A_2(3p_y)\}\rangle \quad \text{(A2)}$$

where α and β are numerical coefficients. $|\alpha|^2$and $|\beta|^2$ give the probability of finding the states described by $|\psi_-\rangle$ and $|\psi_+\rangle$ in the $|\phi_1\{0_0^0(a_1),{}^1B_1(3p_z)\}\rangle$ and $|\phi_2\{9_0^1(b_2),{}^1A_2(3p_y)\}\rangle$ components. The band intensity, I, is proportional to the square of the matrix element between the initial and final wave functions:

$$I \sim \mu_{el}{}^2|\langle\psi_{\nu'}|\psi_{\nu''}\rangle|^2 \quad \text{(A3)}$$

where μ_{el} is the electronic transition dipole moment from the initial to the final vibronic state, and $\psi_{\nu''}$ and $\psi_{\nu'}$ are the nuclear wave functions of the initial and final states, respectively.

Thus, the intensities of transitions from the $|\psi_-\rangle$ state to $\nu^+ = 0$ and 1 states of the cation are:

$$I_1 \sim \mu_{i,3pz}{}^2|\langle\psi_{\nu^+=0}|\psi_-\rangle|^2 = \mu_{i,3pz}{}^2|\beta|^2 \quad \text{(A4)}$$

$$I_2 \sim \mu_{i,3py}{}^2|\langle\psi_{\nu^+=1}|\psi_-\rangle|^2 = \mu_{i,3py}{}^2|\alpha|^2 \quad \text{(A5)}$$

respectively. $\mu_{i,3py}$and $\mu_{i,3pz}$ are the electronic transition dipole moments from the $2^1A_2(3p_y \leftarrow \pi)$ and $2^1B_1(3p_z \leftarrow \pi)$ Rydberg states to the $1^2B_1(\infty \leftarrow \pi)$ cation state, and ψ_{ν^+} is the nuclear wave function of the cation. Likewise, the intensities of transitions from the $|\psi_+\rangle$ state to $\nu = 0$ and 1 states of the cation are:

$$I_3 \sim \mu_{i,3pz}{}^2|\langle\psi_{\nu^+=0}|\psi_+\rangle|^2 = \mu_{i,3pz}{}^2|\alpha|^2 \quad \text{(A6)}$$

$$I_4 \sim \mu_{i,3py}{}^2|\langle\psi_{\nu^+=1}|\psi_+\rangle|^2 = \mu_{i,3py}{}^2|\beta|^2 \quad \text{(A7)}$$

respectively.

The similarity in the geometries (Figure 2) and electronic core structures of the $2^1A_2(3p_y \leftarrow \pi)$ and $2^1B_1(3p_z \leftarrow \pi)$ Rydberg states and the $1^2B_1(\infty \leftarrow \pi)$ cation state (Table 2) result in a strong propensity for ionization via diagonal ($\Delta\nu = 0$) transitions. In addition, the quantum defects of the $3p_z$ and $3p_y$ electronic states are similar and typical of a Rydberg states. As no state-specific selection rules are expected in the ionization from these states to the cation continuum, we assume that the electronic transition dipole moments for the two transitions are very similar.

Therefore, from the eKE distributions at $\lambda = 380.75$ nm (52 528 cm^{-1}) and assuming that $\mu_{i,3py} = \mu_{i,3pz}$ we obtain:

$$\frac{I_2}{I_1} = \frac{|\alpha|^2}{|\beta|^2} = 1.85 \quad \text{(A8)}$$

and from the eKE distributions at $\lambda = 379.50$ nm (52 700 cm^{-1}):

$$\frac{I_3}{I_4} = \frac{|\alpha|^2}{|\beta|^2} = 1.79 \quad \text{(A9)}$$

giving an average value of $|\alpha|^2/|\beta|^2 = 1.82$. Using $|\alpha^2| + |\beta^2| = 1$, we obtain $\alpha = 0.8$ and $\beta = 0.6$. To find the unperturbed energy levels the equations below have been solved for $E_- =$

52 528 cm^{-1} (9^1_0,$2^1A_2(3p_y \leftarrow \pi)$); $E_+ = 52\ 700\ cm^{-1}$ (0^0_0,2^1B_1-$(3p_z \leftarrow \pi)$):

$$E_- = \frac{1}{2}(E_1 + E_2) - \frac{1}{2}\sqrt{(E_1 - E_2)^2 + 4V_{12}^2} \quad \text{(A10)}$$

$$E_+ = \frac{1}{2}(E_1 + E_2) + \frac{1}{2}\sqrt{(E_1 - E_2)^2 + 4V_{12}^2} \quad \text{(A11)}$$

$$\frac{2V_{12}}{E_1 - E_2} = \frac{2\frac{\alpha}{\beta}}{1 - \frac{\beta^2}{\alpha^2}} \quad \text{(A12)}$$

The solution is: $E_1 = 52\ 638\ cm^{-1}$; $E_2 = 52\ 590\ cm^{-1}$; $V_{12} \sim 83\ cm^{-1}$.

References and Notes

(1) Kirmse, W., Ed. *Carbene Chemistry*; Academic Press: New York, 1971.

(2) Raulin, F.; Khlifi, M.; Dang-Nhu, M.; Gautier, D. *Adv. Space Res.* **1992**, *12*, 181.

(3) Kirkbride, F. W.; Norrish, R. G. W. *J. Chem. Soc.* **1933**, 119.

(4) Okabe, H. *Photochemistry of Small Molecules*; Wiley: New York, 1978.

(5) Walch, S. P.; Goddard, W. A., III. *J. Am. Chem. Soc.* **1975**, *97*, 5319.

(6) Bastide, J.; Maier, J. P. *Chem. Phys.* **1976**, *12*, 177.

(7) Herzberg, G. *Proc. R. Soc. London, Ser. A* **1961**, *262*, 291.

(8) Herzberg, G. *Molecular Spectra and Molecular Structure: Electronic Spectra and Electronic Structure of Polyatomic Molecules*; van Nostrand Reinhold: New York, 1966; Vol. III.

(9) Habas, M.; Dargelos, A. *Chem. Phys.* **1995**, *199*, 177.

(10) Brinton, R. K.; Volman, D. H. *J. Chem. Phys.* **1951**, *19*, 1394.

(11) Wolf, R. J.; Hase, W. L. *J. Phys. Chem.* **1978**, *82*, 1850.

(12) Merer, A. J. *Can. J. Phys.* **1964**, *42*, 1242.

(13) McKay, A. F.; Wright, G. F. *J. Am. Chem. Soc.* **1947**, *69*, 3028.

(14) McKay, A. F. *J. Am. Chem. Soc.* **1948**, *70*, 1974.

(15) Sanov, A.; Droz-Georget, T.; Zyrianov, M.; Reisler, H. *J. Chem. Phys.* **1997**, *106*, 7013.

(16) Dribinski, V. Ph.D. Thesis. The University of Southern California, Los Angeles, Califonia, 2004.

(17) Moore, C. B.; Pimentel, G. C. *J. Chem. Phys.* **1964**, *40*, 329.

(18) Khlifi, M.; Paillous, P.; Bruston, P.; Raulin, F.; Guillemin, J. C. *Icarus* **1996**, *124*, 318.

(19) Eppink, A. T. J. B.; Parker, D. H. *Rev. Sci. Instrum.* **1997**, *68*, 3477.

(20) Tanaka, Y.; Kawasaki, M.; Matsumi, Y.; Fujiwara, H.; Ishiwata, T.; Rogers, L. J.; Dixon, R. N.; Ashfold, M. N. R. *J. Chem. Phys.* **1998**, *109*, 1315.

(21) Chang, B.-Y.; Hoetzlein, R. C.; Mueller, J. A.; Geiser, J. D.; Houston, P. L. *Rev. Sci. Instrum.* **1998**, *69*, 1665.

(22) Dribinski, V.; Ossadtchi, A.; Mandelshtam, V. A.; Reisler, H. *Rev. Sci. Instrum.* **2002**, *73*, 2634.

(23) Raghavachari, K.; Trucks, G. W.; Pople, J. A.; Head-Gordon, M. *Chem. Phys. Lett.* **1989**, *157*, 479.

(24) Watts, J. D.; Gauss, J.; Bartlett, R. J. *J. Chem. Phys.* **1993**, *98*, 8718.

(25) Dunning, T. H. *J. Chem. Phys.* **1989**, *90*, 1007.

(26) Becke, A. D. *J. Chem. Phys.* **1993**, *98*, 5648.

(27) Koch, H.; Jensen, H. J. Aa.; Jørgensen, P.; Helgaker, T. *J. Chem. Phys.* **1990**, *93*, 3345.

(28) Stanton, J. F.; Bartlett, R. J. *J. Chem. Phys.* **1993**, *98*, 7029.

(29) Krishnan, R.; Binkley, J. S.; Seeger, R.; Pople, J. A. *J. Chem. Phys.* **1980**, *72*, 650.

(30) McLean, A. D.; Chandler, G. S. *J. Chem. Phys.* **1980**, *72*, 5639.

(31) Helgaker, T.; Jørgensen, P.; Olsen, J. *Molecular Electronic Structure Theory*; John Wiley & Sons: New York, 2000.

(32) Hirata, S.; Nooijen, M.; Bartlett, R. J. *J. Chem. Phys.* **2000**, *326*, 255.

(33) Koziol, L.; Levchenko, S.; Krylov, A. I. *J. Phys. Chem. A* **2006**, *110*, 2746.

(34) Schaftenaar, G.; Noordik, J. H. *J. Comput.-Aided Mol. Des.* **2000**, *14*, 123.

(35) Shao, Y.; Molnar, L. F.; Jung, Y.; Kussmann, J.; Ochsenfeld, C.; Brown, S.; Gilbert, A. T. B.; Slipchenko, L. V.; Levchenko, S. V.; O'Neil, D. P.; Distasio, R. A., Jr.; Lochan, R. C.; Wang, T.; Beran, G. J. O.; Besley, N. A.; Herbert, J. M.; Lin, C. Y.; Van Voorhis, T.; Chien, S. H.; Sodt, A.; Steele, R. P.; Rassolov, V. A.; Maslen, P.; Korambath, P. P.; Adamson, R. D.; Austin, B.; Baker, J.; Bird, E. F. C.; Daschel, H.; Doerksen, R. J.; Drew, A.; Dunietz, B. D.; Dutoi, A. D.; Furlani, T. R.; Gwaltney, S. R.; Heyden, A.; Hirata, S.; Hsu, C.-P.; Kedziora, G. S.; Khalliulin, R. Z.; Klunziger, P.; Lee, A. M.; Liang, W. Z.; Lotan, I.; Nair, N.; Peters, B.; Proynov, E. I.; Pieniazek, P. A.; Rhee, Y. M.; Ritchie, J.; Rosta, E.; Sherrill, C. D.; Simmonett, A. C.; Subotnik, J. E.; Woodcock, H. L., III; Zhang, W.; Bell, A. T.; Chakraborty, A. K.; Chipman, D. M.; Keil, F. J.; Warshel, A.; Herhe, W. J.; Schaefer, H. F., III; Kong, J.; Krylov, A. I.; Gill, P. M. W.; Head-Gordon, M. *Phys. Chem. Chem. Phys.* **2000**, *8*, 3172.

(36) Stanton, J. F.; Gauss, J.; Watts, J. D.; Lauderdale, W. J.; Bartlett, R. J. *ACES II*, 1993. The package also contains modified versions of the MOLECULE Gaussian integral program of J. Almlöf and P. R. Taylor, the ABACUS integral derivative program written by T. U. Helgaker, H. J. Aa. Jensen, P. Jørgensen, and P. R. Taylor, and the PROPS property evaluation integral code of P. R. Taylor.

(37) Arnold, D. W. Ph.D. Thesis. The University of California, Berkeley, Califonia, 1994.

(38) Dunning, T. H.; Hay P. J. In *Modern Theoretical Chemistry*; Plenum Press: New York, 1977.

(39) Sinha, D.; Mukhopadhyay, D.; Mukherjee, D. *Chem. Phys. Lett.* **1986**, *129*, 369.

(40) Sinha, D.; Mukhopadhyay, D.; Chaudhuri, R.; Mukherjee, D. *Chem. Phys. Lett.* **1989**, *154*, 544.

(41) Chaudhuri, R.; Mukhopadhyay, D.; Mukherjee, D. *Chem. Phys. Lett.* **1989**, *162*, 393.

(42) Rabalais, J. W.; McDonald, J. R.; Scherr, V. M.; McGlynn, S. P. *Chem. Rev.* **1971**, *71*, 73.

(43) Glendening, E. D.; Badenhoop, J. K.; Reed, A. E.; Carpenter, J. E.; Bohmann, J. A.; Morales, C. M.; Weinhold, F. *NBO 5.0*; Theoretical Chemistry Institute, University of Wisconsin: Madison, WI, 2001.

(44) Lim, E. C., Ed. *Excited States*; Academic Press: New York, 1966; Vol. III.

(45) Moore, C. B. *J. Chem. Phys.* **1963**, *39*, 1884.